www.czasopisma.pan.pl PAN www.journals.pan.pl
Opto-Electronics Review 25 (2017) 171–180

Contents lists available at ScienceDirect

Opto-Electronics Review

journal homepage: http://www.journals.elsevier.com/opto-electronics review

Current status of modelling the semi-insulating 4H–SiC transient photoconductivity for application to photoconductive switches

M. Suproniuk[a,*], P. Kamiński[b], R. Kozłowski[b], M. Pawłowski[a], M. Wierzbowski[a]

[a] Military University of Technology, ul. Kaliskiego 2, 00-908 Warszawa, Poland
[b] Institute of Electronic Materials Technology, ul. Wólczyńska 133, 01-919 Warszawa, Poland

ARTICLE INFO

Article history:
Received 27 January 2017
Received in revised form 22 March 2017
Accepted 24 March 2017
Available online 9 May 2017

Keywords:
Transient photoconductivity
Modelling
Semi-insulating 4H–SiC
Photoconductive switch

ABSTRACT

In this paper we present the current status of modelling the time evolution of the transient conductivity of photoexcited semi-insulating (SI) 4H–SiC taking into account the properties of defect centres. A comprehensive model that includes the presence of six, the most significant, point defects occurring in SI 4H–SiC crystals is presented. The defect centres are attributed to the two kinds of nitrogen-related shallow donors, a boron-related shallow acceptor, deep electron and hole traps, and the $Z_{1/2}$ recombination centre. We present the results of the state-of-the-art numerical simulations showing how the photoconductivity transients change in time and how these changes are affected by the properties of defect centres. The properties of defect centres assumed for modelling are compared with the results of experimental studies of deep-level defects in high purity (HP) SI 4H–SiC wafers performed by the high-resolution photoinduced transient spectroscopy (HRPITS). The simulated photoconductivity transients are also compared with the experimental photocurrent transients for the HP SI 4H–SiC wafers with different deep-level defects. It is shown that a high-temperature annealing producing the C-rich material enables the fast photocurrent transients to be achieved. The presented analysis can be useful for technology of SI 4H–SiC high-power photoconductive switches with suitable characteristics.

1. Introduction

Recently developed wide-band-gap semi-insulating semiconductor materials like GaAs [1,2], GaN [3–5] or SiC [3,6–8] are used in the production of new semiconductor devices. One kind of such devices are photoconductive semiconductor switches (PCSSs). A superior material for its applications in electricity transfer equipment requiring high voltage and high speed is 4H–SiC. Devices made of the material are characterized by photoconductivity rise times of 1–10 ns and are capable of blocking DC electric fields above 500 kV cm^{-1} as well as switching 20 kV at 250 A [9]. It is worth adding that devices made of SI 4H–SiC can work at higher temperatures, up to ~300 °C.

At present, for device manufacturing, high-purity semi-insulating (HPSI) 4H–SiC single crystals grown by physical vapour deposition (PVT) or high temperature chemical vapour deposition (HTCVD) are used [10,11]. The high resistivity of this material at room temperature may be in the range of 10^7–10^{11} Ω cm and it is achieved by defect engineering resulting in reducing the concentrations of shallow donors and shallow acceptors and introducing native deep-level defects whose concentrations are controlled by the crystal growth conditions. The well-known deep electron trap in 4H–SiC is the $Z_{1/2}$ centre with an activation energy for electron emission of ~0.63 eV. The concentration of this centre is dependent on the crystal stoichiometry and in C-rich crystals is substantially reduced. The $Z_{1/2}$ defect is an amphoteric negative-*U* centre having the donor (0/+) level located closer to the conduction band minimum than the acceptor level (−/0) [12,13]. The experimentally observed electron thermal emission to the conduction band occurs from an effective acceptor level located between the two levels. Apart from the $Z_{1/2}$ centre, a number of other deep defect centres with activation energies ranging from 560 to 1530 meV that may be involved in the charge compensation have been observed in SI 4H–SiC [14]. The observed deep centres are mainly associated with carbon vacancies (V_C), silicon vacancies (V_{Si}), carbon antisite–vacancy pairs and divacancies V_CV_{Si} [15].

For applications in photoconductive switches it is necessary to know how physical properties of the material, like doping and defects parameters, affect electrical properties of the final device.

* Corresponding author.
E-mail addresses: marek.suproniuk@wat.edu.pl (M. Suproniuk), pawel.kaminski@itme.edu.pl (P. Kamiński).

http://dx.doi.org/10.1016/j.opelre.2017.03.006
1896-3757/

For this purpose, a dedicated numerical simulation is very useful. A literature review shows that significant information is present in time evolution of the material's photoconductivity following its illumination, which has been observed both experimentally and as computer simulations [6,9,16–19]. It has been shown that the photoconductivity transients can be of various shapes which are dependent on the defect centres properties [20,21]. Typically, the simulations consist of numerical solutions to the continuation equations, as well as equations describing processes of band-to-band transitions of charge carriers (generation and recombination) and processes of exchange of the carriers between defect centres levels and conduction and valence bands (trap occupancy models). However, models on which the simulations are based consider only a small number of defect centres, and the effect of capture and emission processes, occurring with the involvement of specific defect centres, have not been studied to explain the changes in photoconductivity as a function of time. Therefore, in this paper we fill the gap for the photoexcited SI 4H–SiC.

For the first time shown is a time evolution of changes in concentration of charge carriers at individual defect levels which was determined based on comprehensive model of the 4H–SiC material [22]. It includes the presence of many defects, six most significant, occurring in actual material, parameters of which were obtained from experimental measurements [23–26]. They involve: two kinds of nitrogen-related shallow donors, a boron-related shallow acceptor, a deep electron trap, a deep hole trap and the $Z_{1/2}$ recombination centre. By performing numerical simulations, the model enables conducting studies of time parameters of photoconductivity transients and changes in photoconductivity alone resulting from different degree of defect levels filling influenced by different values of the material's parameters. It allows also to correlate time changes of excess electrons and holes concentrations in the conduction and valence bands, respectively, with rates of capture of excess charge carriers by defect centres and with rates of thermal emission of the carriers from defect levels to the bands.

The demonstrated simulator can be used not only for designing the high-power PCSSs, but also it can represent a module of a diagnostic system used for the characterization of defect centres and determination of their concentrations [27,28].

2. Defect centres and material properties

Fig. 1 shows positions of energy levels in the SI 4H–SiC band gap attributed to the main known defect centres that take part in the charge compensation resulting in the material's semi-insulating properties [22]. Among these defect centres there are the two kinds of shallow donors (SD1 and SD2) attributed to nitrogen, the shallow acceptor (SA) attributed to boron, the deep electron trap (ET) associated with the known ID9 centre, the deep hole trap (HT) associated with the known HK3 centre and the recombination centre (RC) related to the $Z_{1/2}$ defect. It is worth noting that in the 4H–SiC lattice there are two inequivalent sites: hexagonal (h) and cubic (k), and point defects located at different sites may have different activation energies.

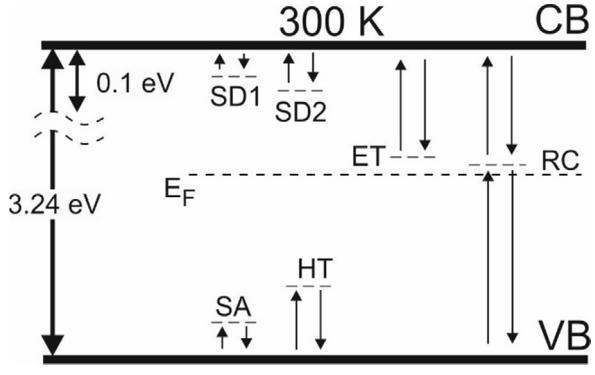

Fig. 1. Illustration of energy levels in the SI 4H–SiC band gap (at 300 K) assumed for the numerical simulations of the photoconductivity time evolution. The labels SD1, SD2, SA, ET, HT, RC and E_F mark levels of two types of shallow donors as well as the levels of shallow acceptor, deep electron trap, deep hole trap, recombination centre and the Fermi level, respectively. The arrows indicate direction of the electron transitions between the levels and the bands. The excess electron–hole pairs are photo-excited through electron transitions from the valence (VB) to conduction (CB) band.

Thus, the shallow donors levels SD1 and SD2 are associated with the nitrogen atoms substituting carbon atoms located at the h and k lattice sites, respectively [23]. As it is shown in Fig. 1, these levels act as the shallow electron traps. The shallow acceptor level (SA), acting as the shallow hole trap, is formed by boron atoms substituting the Si atoms located either at the h or k lattice sites [23]. The ID9 deep electron trap (ET level) is presumably related to a carbon vacancy (V_C) [23] and the HK3 deep hole trap (HT level) can be tentatively identified with a silicon vacancy (V_{Si}) [24]. It should be noted that the HK3 centre, observed by deep level transient spectroscopy (DLTS), is probably related to the same defect, known as the ID centre, whose properties were studied by electron paramagnetic resonance (EPR) [25]. In view of the results of our previous studies, the $Z_{1/2}$ centre is likely to be formed by the two types of divacancies: a divacancy involving carbon vacancy at the h site and silicon vacancy at the k site ($V_C{}^hV_{Si}{}^k$) as well as a divacancy involving carbon vacancy at the k site and silicon vacancy at the h site ($V_C{}^kV_{Si}{}^h$) [23,26]. The properties of defect centres introducing these levels are listed in Table 1.

The Fermi level position in the band gap as a function of temperature is calculated by solving the charge neutrality equation:

$$n_0 - N^+_{SD1} - N^+_{SD2} - N^+_{ET} = p_0 - N^-_{SA} - N^-_{RC} - N^-_{HT} \quad (1)$$

where n_0 and p_0 are equilibrium concentrations of electrons and holes, N^+_{SD1}, N^+_{SD2} and N^+_{ET} are the concentrations of ionized SD1, SD2 and ET donors, N^-_{SA}, N^-_{HT} and N^-_{RC} are concentrations of ionized acceptors SA, HT and RC, assuming that N_{SD}, N_{SA}, N_{ET}, N_{HT} and N_{RC} are the total concentrations of shallow donors, shallow acceptors, electron traps, hole traps and recombination centres, respectively.

Calculated from the neutrality Eq. (1) the Fermi level at 300 K with respect to the top of the valence band is equal to $E_F = 2.536$ eV. The concentration of electrons in the conduction band is equal to $n_0 = 3.03 \times 10^7$ cm^{-3}, and the holes concentration in the valence band is approximately equal to zero. Assuming that the mobilities of electrons and holes equal $\mu_n = 950$ cm^2 V^{-1} s^{-1} and $\mu_p = 150$ cm^2 V^{-1} s^{-1}, respectively, it was calculated that the dark conductivity of the material is $\sigma_0 = 4.62 \times 10^{-9}$ Ω^{-1} cm^{-1}, corresponding to resistivity $\rho = 2.16 \times 10^8$ Ω cm. The concentrations of electrons occupying the energy levels in the bandgap are also calculated using the neutrality equation. The equilibrium concentration of electrons at the levels SD1 and SD2 are $n_{SD1} = 1.23 \times 10^5$ cm^{-3} and $n_{SD2} = 6.26 \times 10^5$ cm^{-3}, respectively, which means that these levels are fully ionized. On the other hand, the levels SA and HT are completely filled with electrons. The equilibrium electron concentration at the ET level is $n_{ET} = 3.73 \times 10^{12}$ cm^{-3} and in the recombination centres RC it is $n_{RC} = 9.63 \times 10^{13}$ cm^{-3}. So, the defect ET is filled at room temperature in 0.7% and the degree of filling the centres RC is 12%.

3. Rate equations

The phenomena associated with the emission and capture of excess electrons and holes by defect centres after switching on the photoexcitation of electron–hole pairs are modelled with the set

Table 1
Defect centres properties assumed for the kinetic simulation of 4H–SiC.

Defect label	Defect type	Capture cross-section (cm^2)		Activation energy (eV)	Concentration(cm^{-3})	Identification
		Electrons	Holes			
SD1	Shallow donor	$\sim 4.0 \times 10^{-20}$	–	$E_c - 0.050$	5×10^{15}	N_C in *h* site [23]
SD2	Shallow donor	$\sim 4.0 \times 10^{-19}$	–	$E_c - 0.092$	5×10^{15}	N_C in *k* site [23]
ET	Electron trap	$\sim 1.2 \times 10^{-15}$	–	$E_c - 0.555$	5×10^{14}	ID9 [23]
RC	Recombination centre	1.3×10^{-14}	1.0×10^{-14}	$E_c - 0.630$	8×10^{14}	$Z_{1/2}$ centre [23,26]
HT	Hole trap	–	$\sim 3.1 \times 10^{-14}$	$E_v + 1.125$	7×10^{14}	ID centre [25], HK3 trap [24]
SA	Shallow acceptor	–	$\sim 3.1 \times 10^{-17}$	$E_v + 0.285$	9.7×10^{15}	B_{Si} in both *h* and *k* sites [23]

of differential-type rate equations The rates of changes in the electron and hole concentrations on the levels of the defect centres are described by equations from (2) to (7). The rate of change in the excess electron concentration in the conduction band and the rate of change in the excess hole concentration in the valence band are described by Eqs. (8) and (9), respectively.

$$\frac{dn_1(t)}{dt} = \underbrace{n(t)c_{SD1}\left(\frac{N_{SD}}{2} - n_1(t)\right)}_{\text{capture}} - \underbrace{e_{SD1}n_1(t)}_{\text{emission}} \tag{2}$$

$$\frac{dn_2(t)}{dt} = \underbrace{n(t)c_{SD2}\left(\frac{N_{SD}}{2} - n_2(t)\right)}_{\text{capture}} - \underbrace{e_{SD2}n_2(t)}_{\text{emission}} \tag{3}$$

$$\frac{dn_3(t)}{dt} = \underbrace{n(t)c_{ET}(N_{ET} - n_3(t))}_{\text{capture}} - \underbrace{e_{ET}n_3(t)}_{\text{emission}} \tag{4}$$

$$\frac{dn_4(t)}{dt} = \underbrace{n(t)c_{RC_n}(N_{RC} - n_4(t))}_{\text{n capture}} - \underbrace{e_{RC_n}n_4(t)}_{\text{n emission}} - \underbrace{p(t)c_{RC_p}n_4(t)}_{\text{p capture}} + \underbrace{e_{RC_p}(N_{RC} - n_4(t))}_{\text{p emission}} \tag{5}$$

$$\frac{dp_1(t)}{dt} = \underbrace{e_{SA}p_1(t)}_{\text{emission}} - \underbrace{p(t)c_{SA}(N_{SA} - p_1(t))}_{\text{capture}} \tag{6}$$

$$\frac{dp_2(t)}{dt} = \underbrace{e_{HT}p_2(t)}_{\text{emission}} - \underbrace{p(t)c_{HT}(N_{HT} - p_2(t))}_{\text{capture}} \tag{7}$$

$$\frac{dn(t)}{dt} = \underbrace{e_{SD1}n_1(t) - n(t)c_{SD1}\left(\frac{N_{SD}}{2} - n_1(t)\right)}_{1} + \underbrace{e_{SD2}n_2(t) - n(t)c_{SD2}\left(\frac{N_{SD}}{2} - n_2(t)\right)}_{2} + \underbrace{e_{ET}n_3(t) - n(t)c_{ET}(N_{ET} - n_3(t))}_{3} + \underbrace{e_{RC_n}n_4(t) - n(t)c_{RC_n}(N_{RC} - n_4(t))}_{4} - \underbrace{\frac{n(t)}{\tau_n}}_{5} + G \tag{8}$$

$$\frac{dp(t)}{dt} = \underbrace{e_{SA}p_1(t) - p(t)c_{SA}(N_{SA} - p_1(t))}_{1} + \underbrace{e_{HT}p_2(t) - p(t)c_{HT}(N_{HT} - p_2(t))}_{2} + \underbrace{e_{RC_p}p_3(t) - p(t)c_{RC_p}(N_{RC} - p_3(t))}_{3} - \underbrace{\frac{p(t)}{\tau_p}}_{4} + G \tag{9}$$

It is worth noting that Eq. (8), which determine the rate of the excess electron concentration change in the conduction band, takes into account the thermal emission rate e and the capture coefficient c of electrons associated with the shallow donor levels SD1 and SD2 (components labelled as 1 and 2, respectively). The processes of electrons exchange between conduction band and the ET and RC levels are described by the components labelled as 3 and 4, respectively, and process of direct band-to-band recombination is described by the component labelled as 5 and the electron–hole pairs generation rate is represented by G.

Eq. (9), in turn, describes the rate of the excess hole concentration change in the valence band and it depends on the exchange rates of holes between the valence band and the centres SA, HT, RC (components labelled as 1, 2 and 3, respectively). Additionally, the concentration of holes in the valence band depends on the recombination process (component labelled as 4) and on the electron–hole pairs generation rate G.

For the time dependent electron concentrations on the levels of defect centres SD1, SD2, ET designations $n_1(t)$, $n_2(t)$ and $n_3(t)$, respectively, were introduced. Similarly, the time dependent hole concentrations on the levels of defect centres SA and HT were designated by $p_1(t)$ and $p_2(t)$, respectively, and the time dependent electron concentration on the recombination level RC is given by $n_4(t)$. The time dependent hole concentration $p_3(t)$ on the recombination centre level included in Eq. (9) is determined by the difference between the concentration of the recombination centres N_{RC} and the electron concentration $n_4(t)$. The rate in the change of the electron concentration $n_4(t)$ is described by Eq. (5) that includes the processes of the thermal emission of electrons to the conduction band and their capture from this band as well as the processes of the thermal emission of holes to the valence band and their capture from this band. All the processes of the capture and the thermal emission and of charge carriers from the defect centres assumed in equations from (2) to (9) are marked in Fig. 1. The parameter that specifies the rate of electrons and holes recombination processes, i.e. lifetime, can be expressed as [29]:

$$\tau_n = \frac{1}{N_{RC}\sigma_n\nu_n}, \tag{10}$$

$$\tau_p = \frac{1}{N_{RC}\sigma_p\nu_p}, \tag{11}$$

where σ_n and σ_p are capture cross-sections for electrons and holes, respectively, and ν_n and ν_p are the mean thermal velocities of electrons and holes, respectively, depending on their effective masses and the temperature, respectively. The rates of electrons and holes

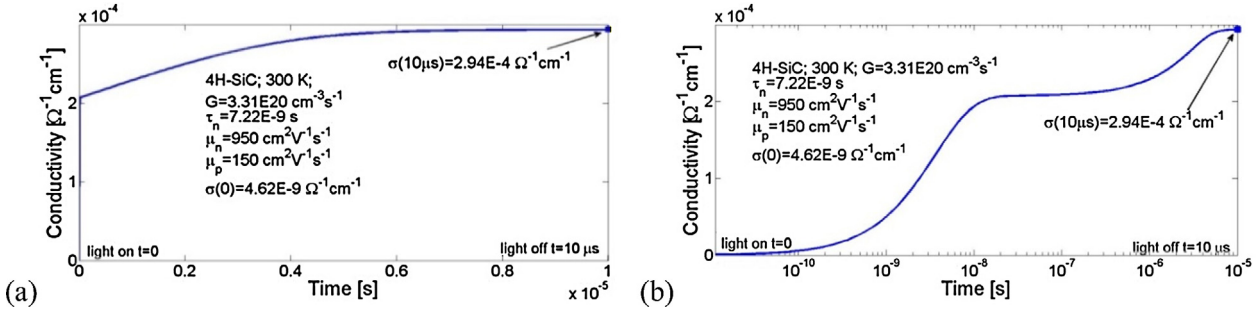

Fig. 2. Time evolution of the SI 4H–SiC photoconductivity simulated for $T = 300$ K and the generation rate of electron–hole pairs $G = 3.31 \times 10^{20}$ cm^{-3}s^{-1} using the proposed model for SI 4H–SiC defect structure. (a) The linear scale for the time axis. (b) The logarithmic scale for the time axis.

capture for a given defect centre are characterized by the capture coefficients c_n and c_p, respectively, given by:

$$c_n = \sigma_n \upsilon_n, \tag{12}$$

$$c_p = \sigma_p \upsilon_p, \tag{13}$$

where σ_n and σ_p are capture cross-sections for electrons and holes, respectively. The thermal emission rates of electrons e_n or holes e_p from a defect centre to the conduction or valence band, respectively, are described by the expressions:

$$e_n = \sigma_n \gamma_n T^2 \exp\left(\frac{-E_{an}}{k_B T}\right), \tag{14}$$

$$e_p = \sigma_p \gamma_p T^2 \exp\left(\frac{-E_{ap}}{k_B T}\right), \tag{15}$$

where T is the absolute temperature, E_{an} is the activation energy relative to the bottom of the conduction band for electrons emission from a defect centre, E_{ap} is the activation energy for holes emission relative to the top of the valence band from a defect centre, and k_B is the Boltzmann constant. The coefficients γ_n and γ_p are dependent on the electron and hole effective masses and are equal 2.5×10^{21} and 3.26×10^{21} cm^{-2} s^{-1} K^{-2}, respectively.

In the simulation process, the set of Eqs. (2)–(9) is numerically solved with MATLAB software using variable time step Runge–Kutta–Fehlberg method.

4. Time evolution of SI 4H–SiC photoconductivity

The time dependent photoconductivity $\sigma(t)$ for semi-insulating materials can be described using the time dependent excess electron concentration in the conduction band $n(t)$ and the time dependent excess hole concentration in the valence band $p(t)$:

$$\sigma(t) = q[\mu_n n(t) + \mu_p p(t)], \tag{16}$$

where q is the elementary charge, and μ_n and μ_p are the electrons and holes mobilities, respectively.

Using the proposed model for the defect structure of SI 4H–SiC, the time evolution of the photoconductivity $\sigma(t)$ was simulated for switching on the photoexcitation with the generation rate of electron–hole pairs $G = 3.31 \times 10^{20}$ cm^{-3} s^{-1} and $T = 300$ K. The transient photoconductivity waveforms are presented in Fig. 2 using the two time scales: the linear one (Fig. 2(a)) and the logarithmic one (Fig. 2(b)). The waveforms showing the photoconductivity evolution in the logarithmic scale are particularly useful for analysing the rise in the conductivity occurring after the very short time from switching on the photoexcitation. This is of great importance for using SI 4H–SiC in high-speed switching systems.

It can be seen from Fig. 2(a) that after 10 μs the photoconductivity transient saturates and the conductivity value stabilizes at $\sigma(10\,\mu s) = 2.94 \times 10^{-4}\ \Omega^{-1}$ cm^{-1}. For this steady condition, the calculated quasi-Fermi levels for electrons and holes are equal to $E_{Fn} = 2.82$ eV and $E_{Fp} = 0.42$ eV with respect to the top of the valence band. The logarithmic scale on the time axis (Fig. 2(b)) reveals in the photoconductivity waveform the presence of two processes. The first one is fast and occurs during the first 20 ns from the moment of switching on the photoexcitation. The second one is much slower and it is visible in the range from 1 to 10 μs after switching on the photoexcitation.

The changes in time of the excess electron concentration in the conduction band are presented in Fig. 3. The waveforms represent the solutions of Eq. (8). The equilibrium electron concentration in the conduction band before photoexcitation is $n(0) = 3.03 \times 10^7$ cm^{-3}. At the steady state seen at $t = 10$ μs from the start of the photoexcitation, the excess electron concentration is $n = 1.61 \times 10^{12}$ cm^{-3}. For comparison, the dotted lines depict a waveform corresponding to the simple model based only on the difference between the generation and recombination rates of electrons characterized by the electron lifetime $\tau_n = 7.22 \times 10^{-9}$ s. The excess electron concentration in accordance with the simple model

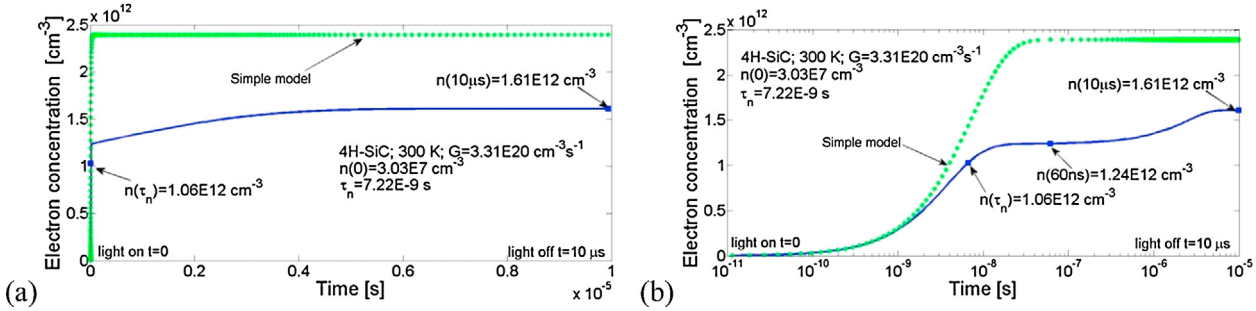

Fig. 3. Time evolution of the excess electron concentration in the conduction band of SI 4H–SiC simulated for $T = 300$ K and the generation rate of electron–hole pairs $G = 3.31 \times 10^{20}$ cm^{-3} s^{-1} using the proposed model for SI 4H–SiC defect structure. (a) The linear scale for the time axis. (b) The logarithmic scale for the time axis. The dotted line depicts the changes of the excess electron concentration in time obtained from the simple model based only on a difference between the generation rate G and the electron recombination rate characterized by the lifetime τ_n.

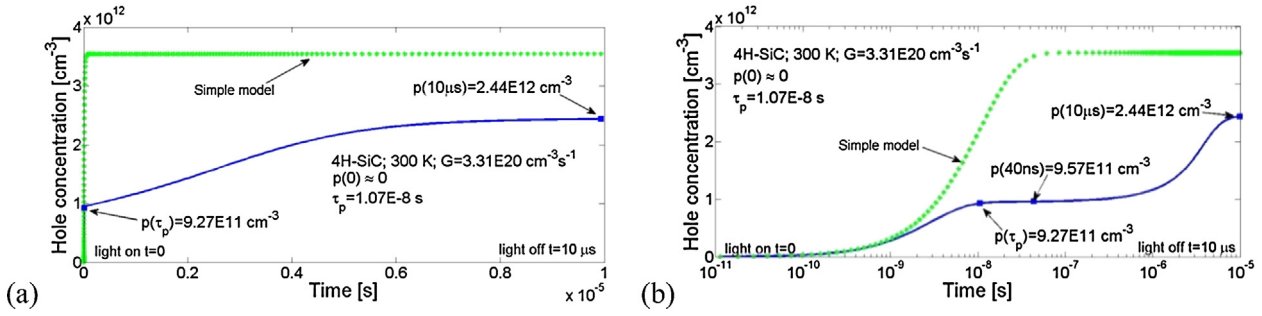

Fig. 4. Time evolution of the excess hole concentration in the valence band of SI 4H–SiC simulated for $T = 300$ K and the generation rate of electron–hole pairs $G = 3.31 \times 10^{20}$ cm^{-3} s^{-1} using the proposed model for SI 4H–SiC defect structure. (a) The linear scale for the time axis. (b) The logarithmic scale for the time axis. The dotted line depicts the changes of the excess hole concentration in time obtained from the simple model based only on a difference between the generation rate G and the hole recombination rate characterized by the lifetime τ_p.

is the product of $G\tau_n$ and after the time $t = 10$ μs it is equal to $n = 2.39 \times 10^{12}$ cm^{-3}. Thus, the excess electron concentration in the conduction band calculated when the proposed model is used is significantly different from that of obtained for the simple model. In other words, the time dependence of the excess electron concentration is strongly affected by the properties and concentrations of defect centres in SI 4H–SiC.

The changes in time of the excess hole concentration in the valence band, determined by the solution of Eq. (9), are presented in Fig. 4. The equilibrium hole concentration in the valence band before the photoexcitation is very close to zero. At the steady state seen at $t = 10$ μs from the start of the photoexcitation, the excess hole concentration is $p = 2.44 \times 10^{12}$ cm^{-3}. Thus, at $t = 10$ μs the excess hole concentration in the valence band is about two times larger than the excess electron concentration in the conduction band. It is worth noting that the in our model the lifetime of holes is 1.07×10^{-8} s and it is significantly longer than that of electrons equal to 7.22×10^{-9} s. The waveform marked with the dotted line depict the results of computations for a simple model, similarly to the changes in the excess electron concentration in the conduction band. The excess hole concentration, as determined by using the simple model, is the product of $G\tau_p$ and at the time of $t = 10$ μs is equal to $p = 3.54 \times 10^{12}$ cm^{-3}. It should be added that the excess electron concentration in the conduction band has the greater impact on the photoconductivity than the excess hole concentration in the valence band. This is due to the fact that the mobility of electrons in SI 4H–SiC is 6.33 times greater than that of holes.

5. Effect of defect centres on the excess electron concentration in the conduction band

Fig. 5 presents the time evolution of the rate of change in the excess electron concentrations related to shallow donor centres SD1 (Fig. 5(a)) and SD2 (Fig. 5(b)) as a result of illumination. Presented waveforms are solutions to Eqs. (2) and (3) and show separately the process of thermal emission of electrons from the defect centres to the conduction band and the process of electrons capture by the defect centres from the conduction band, as well as the resultant behaviour. The exchange of electrons between the conduction band and the defect centres acts differently for the thermal emission and for the capture process. It can be seen, that for both defect centres the first process to appear is the capture process, which after a time of about 10 ns reaches the equilibrium state temporally. Next, after a time of about 100 ns the influence of thermal emission of electrons from the defect centres and further increase in the rate of capture can be seen. Eventually, after several microseconds the capture and thermal emission processes reach the same rate level (mutual balance).

Fig. 6 presents the time evolution of concentrations of electrons trapped in the shallow donor centres SD1 and SD2. They correspond to the waveforms shown in Fig. 5. Again, after a time of $t = 10$ μs the processes of capture and thermal emission of electrons are in a balance and the changes in electrons concentration reach a steady state. After applying the photoexcitation, electron concentration on the level SD1 at the time of $t = 10$ μs is equal to 3.28×10^9 cm^{-3} and on the level SD2 it is equal to 1.66×10^{10} cm^{-3}. It can be seen that the illumination resulted in a minimum filling of traps SD1 and SD2, by even less than 0.001%.

Presented in Fig. 7 are the exchange rates of charge carriers at level ET and in recombination centres RC. The rate of electrons

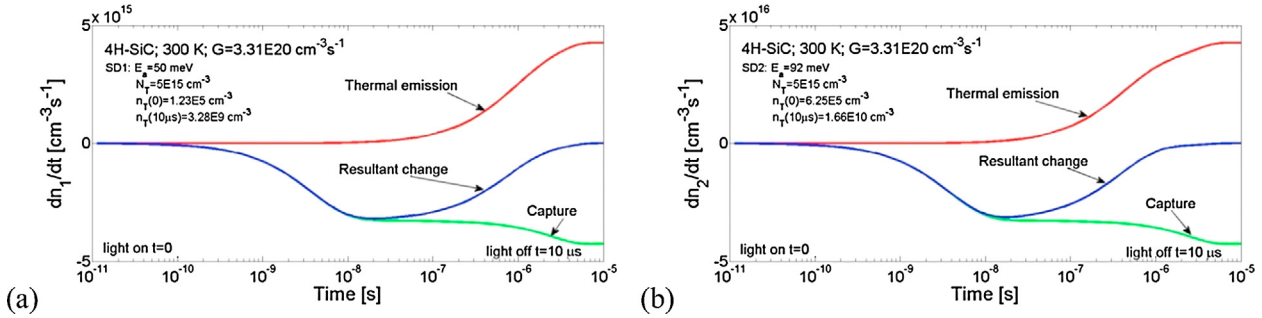

Fig. 5. The time dependences of the rates of changes in the excess electron concentrations resulting from the exchange of electrons between the conduction band and the SD1 (a) and SD2 (b) shallow defect centres. The effects of the thermal emission of electrons to the conduction band and the capture of electrons from the conduction band are demonstrated.

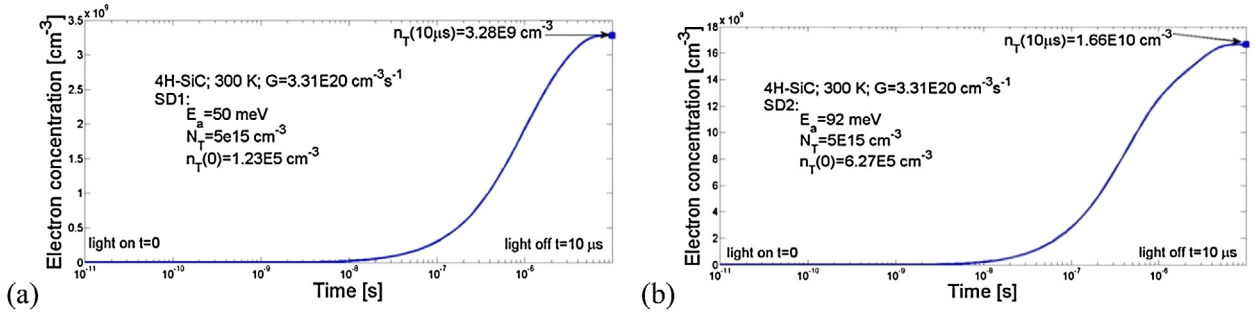

Fig. 6. Time evolution of the concentration of electrons captured by the shallow donor centres SD1 (a) and SD2 (b) as a result of photoexcited electron–hole pairs generation.

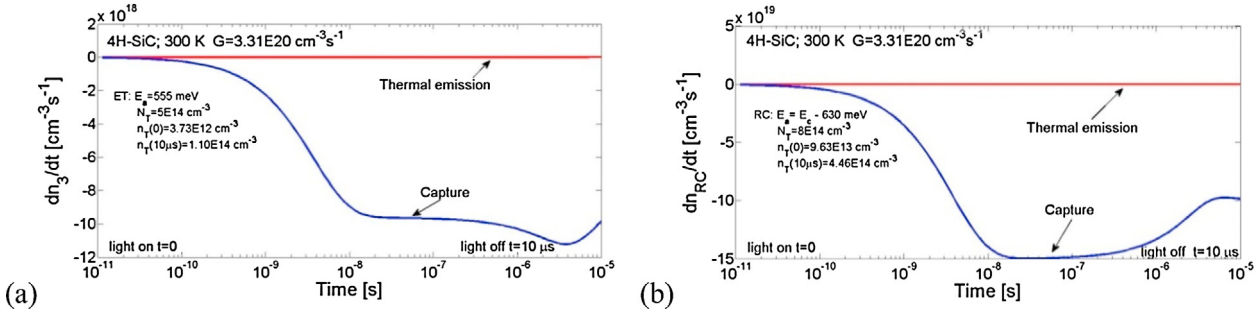

Fig. 7. The time dependences of the rates of changes in the excess electron concentrations resulting from the exchange of electrons between the conduction band and the ET trap (a) and recombination centre RC (b). The effects of the thermal emission of electrons to the conduction band and the capture of electrons from the conduction band are demonstrated.

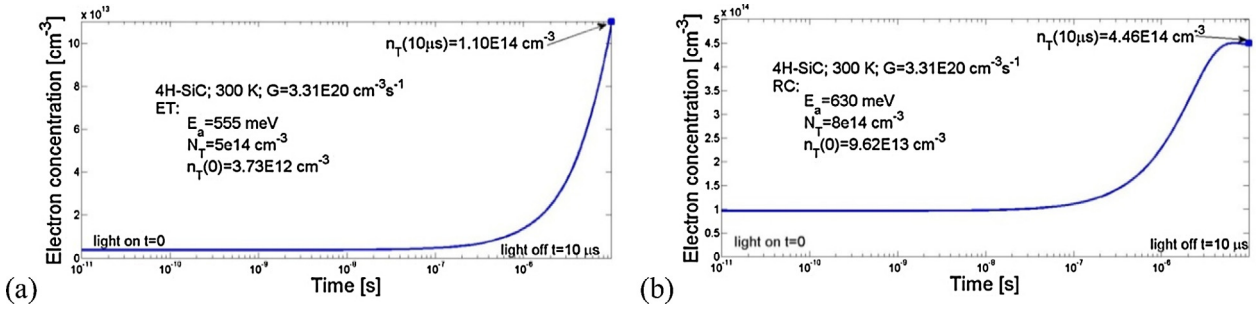

Fig. 8. Time evolution of the concentration of electrons captured by the deep electron trap ET (a) and the recombination centre RC (b) as a result of photoexcited electron–hole pairs generation.

exchange between the conduction band and the recombination centres is described by the first two components of Eq. (5). Presented waveforms show only a process of electrons capture from the conduction band. The process of thermal emission of electrons is negligibly small.

Fig. 8(a) shows a time evolution of concentration of electrons trapped in the ET trap following the illumination. The waveform was obtained by solving Eq. (4). In the analyzed case, the illumination increases the concentration of electrons in the trap to a value of ca. 1.1×10^{14} cm^{-3}, which means that the trap is filled by only 22%. Much higher occupation of the ET defects compared to the occupation of the shallow donors SD1 and SD2 is caused by almost 4 orders of magnitude smaller the coefficient of thermal emission of electrons from the electron trap defect centres into the conduction band and ca. 5 orders of magnitude greater the coefficient of electrons capture from the conduction band. The coefficients are equal to 126 s^{-1} for the thermal emission and to 1.57×10^{-8} cm^3 s^{-1} for the capture process.

The time evolution of concentration of electrons trapped in the recombination centre RC during the generation of electron–hole pairs is presented in Fig. 8(b). The waveform was obtained by solving Eq. (5). In the analyzed case, illumination increases the concentration of electrons in the trap to a value of 4.46×10^{14} cm^{-3}, which means that the trap is filled by over 50%.

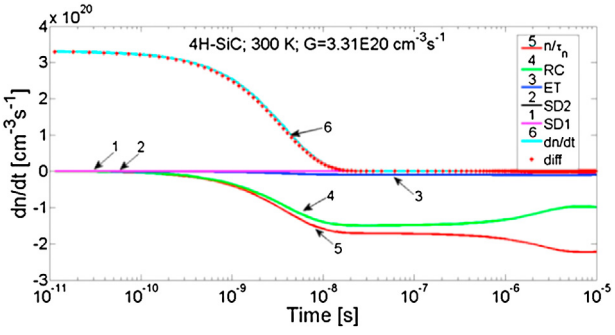

Fig. 9. The contribution of the individual defect centres SD1, SD2, ET, RC (lines 1, 2, 3, and 4, respectively) and the electron recombination rate n/τ_n (line 5) to the time evolution of the rate of changes in the excess electron concentration in the conduction band (line 6). The dotted line marked "diff", fitting very well to the line 6, has been obtained by numerically differentiating the electrons concentration in the conduction band shown in Fig. 3.

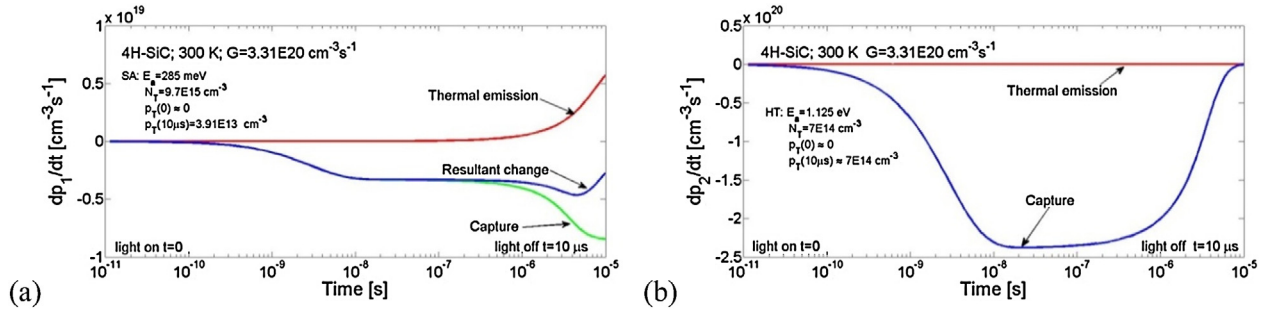

Fig. 10. The time dependences of the rates of changes in the excess hole concentrations resulting from the exchange of holes between the valence band and the shallow acceptor SA (a) and deep hole trap HT (b) centres. The effects of the thermal emission of holes to the valence band and the capture of holes from the valence band are demonstrated.

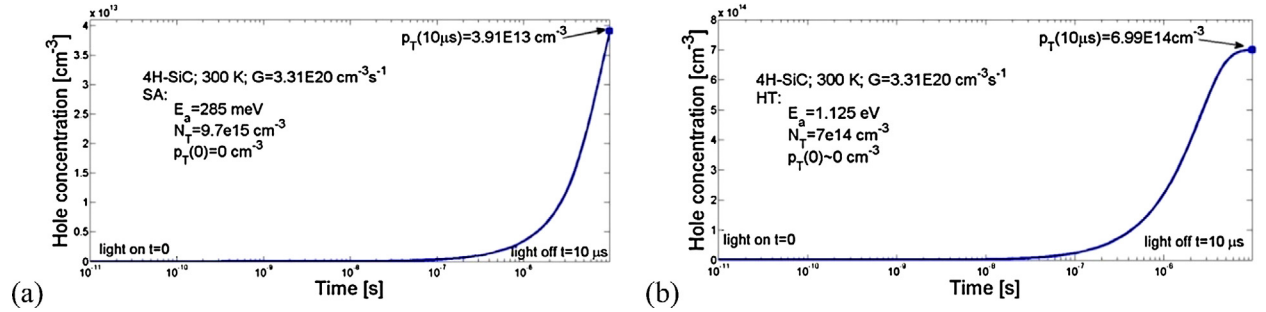

Fig. 11. Time evolution of the concentration of holes captured by the shallow acceptor SA (a) and deep acceptor HT (b) traps as a result of photoexcited electron–hole pairs generation.

Fig. 9 shows the contribution of the individual defect centres SD1, SD2, ET, RC and the electron recombination rate n/τ_n to the time evolution of the rate of changes in the excess electron concentration in the conduction band. The individual waveforms show the rate of exchange of charge carriers between the conduction band and the respective defect centre. Waveforms labelled as 1, 2, 3 and 4 correspond to processes associated with the centres SD1, SD2, ET and RC, respectively, and the waveform labelled as 5 corresponds to the process of band-to-band recombination. The waveform labelled as 6 shows the rate of change in electron concentration in the conduction band as described by Eq. (8), wherein the waveforms' numeration correspond to the components' numeration in the equation. The label "diff" marks the waveform which was obtained by numerically differentiating the excess electron concentration waveform shown in Fig. 3. The calculation was performed to validate the solution of kinetics equations. One can notice a strict accordance of the waveform and the solution labelled as 6.

As can be seen, the processes of exchange of charge carriers between the conduction band and the recombination centre (line 4) and the processes of the band-to-band recombination (line 5) have the greatest influence on the rate of change of electrons concentration in the conduction band.

6. Effect of defect centres on the excess hole concentration in the valence band

The time evolution of the rate change in the excess hole concentrations related to shallow acceptor trap SA was presented in Fig. 10(a). At the beginning the rate is affected by a process of carriers capture by the centre. At a time of a few microseconds the rate of holes capture increases and the process of thermal emission of holes exchange from the shallow acceptor to the valence band takes place.

The rate of exchange of charge carriers between the hole trap HT and the valence band (Fig. 10(b)) depends on a process of carriers capture by this centre from the valence band. The processes of thermal emission of charge carriers from the defect centre to the valence band can be omitted.

The resultant change in concentration of holes in the shallow acceptor trap SA described by Eq. (6) is presented in Fig. 11(a). The hole concentration at the steady state at a time of $t = 10\,\mu s$, under the influence of illumination, increased to $\sim 3.9 \times 10^{13}\,cm^{-3}$. Similarly, Fig. 11(b) presents the increase in the concentration of holes in the hole trap HT obtained by solving Eq. (7). In this case, the illumination increases the concentration of holes to a value of $6.99 \times 10^{14}\,cm^{-3}$, which means that the trap is filled by 99%. Much higher occupation of the HT defect compared to the occupation of the shallow acceptor trap SA is caused by 11 orders of magnitude smaller the coefficient of the thermal emission of electrons from the hole trap defect centres into the valence band and by ca. 3 orders of magnitude greater the coefficient of the holes capture from the valence band. The coefficient of thermal emission of holes from the defect centre HT is equal to $\sim 1 \times 10^{-6}\,s^{-1}$, whereas the coefficient of holes capture is equal to $\sim 4 \times 10^{-7}\,cm^3\,s^{-1}$.

The process of holes exchange between the recombination centre RC and the valence band described by the last two components of Eq. (5) is presented in Fig. 12. As can be seen, only the process of holes capture from the valence band occurs, whilst the process of thermal emission of holes is negligibly small.

Fig. 13 shows the contribution of the individual defect centres SA, HT, RC, and the hole recombination rate p/τ_p to the time evolution of the rate of changes in the excess hole concentration in the valence band. The individual waveforms show the rate of exchange of charge carriers between the valence band and the respective defect centre. Waveforms labelled as 1, 2 and 3 correspond to processes associated with the centres SA, HT and RC, respectively, and the waveform labelled as 4 corresponds to the process of band-to-

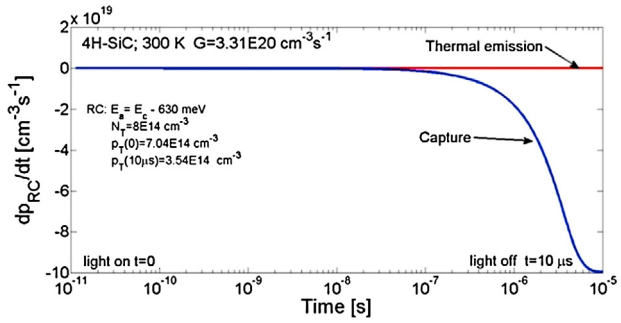

Fig. 12. The time dependency of the rate of change in the excess hole concentration resulting from the exchange of holes between the valence band and the recombination centre RC. The effects of the thermal emission of holes to the valence band and the capture of holes from the valence band are demonstrated.

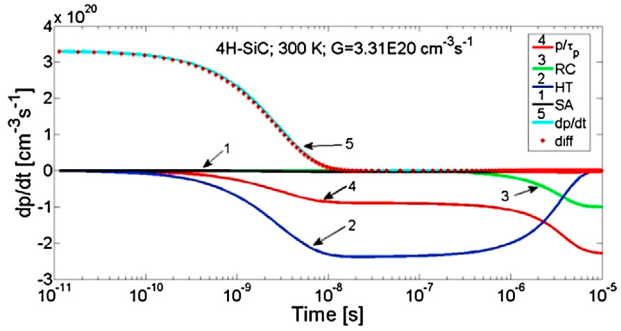

Fig. 13. The contribution of the individual defect centres SA, HT, RC (lines 1, 2 and 3, respectively) and the hole recombination rate p/τ_p (line 4) to the time evolution of the rate of changes in the excess hole concentration in the valence band (line 5). The dotted line marked "diff", fitting very well to the line 5, has been obtained by numerically differentiating the holes concentration in the valence band shown in Fig. 4.

band recombination. The waveform labelled as 5 shows the rate of change in hole concentration in the valence band as described by Eq. (9), wherein the waveforms' numeration correspond to the components' numeration in the equation. The label "diff" marks the waveform which was obtained by numerically differentiating the excess hole concentration waveform shown in Fig. 4. The calculation was performed to validate the solution of kinetics equations. One can notice a strict accordance of the waveform and the solution labelled as 5.

As can be seen, in the first 100 picoseconds from start of illumination the rate of change in the hole concentration in the valence band is equal to the rate of electron–hole pairs generation *G*. After that time, the processes of carriers exchange associated with the centre HT and with the direct band-to-band recombination, takes place. After a few microseconds additional process of exchange – from the recombination centre RC – is visible. At the same time, an increase in the rate of direct band-to-band carriers exchange and a decrease in the rate of carriers exchange between the HT centre and the valence band, can be seen. At a time of $t = 10\,\mu s$ the latter drops down to zero.

7. Comparison with experimental results

The time evolution of the SI 4H–SiC photoconductivity can be observed experimentally by measurements of the photocurrent pulses generated by UV excitation pulses. To show the importance of the performed simulations on understanding the effect of deep-level defects on the rise of the photocurrent pulse after switching on the UV excitation, we present the results of measurements made on two SI 4H–SiC wafers, labelled as wafers A and B, having a different defect structure. The both wafers were prepared from an undoped SI 4H–SiC single crystal with a resistivity at room temperature of $\sim 10^8\ \Omega$ cm. The wafers were cut out perpendicularly to the *c* axis (⟨0001⟩ direction) with the surface polished on the both sides according to the requirements for epitaxial substrates. The wafers' thickness was ~400 μm. The properties and concentrations of deep-level defects were studied in the near surface region of the wafers using the high-resolution photoinduced transient spectroscopy (HRPITS) [14]. The studies were made on the C-face side of the wafers. The wafer A was a typical substrate wafer, while the wafer B was subjected to the heat treatment at ~1670 °C performed in a CVD reactor using the conditions preceding the growth of the epitaxial graphene.

For the HRPITS measurements, arrays of two co-planar ohmic contacts with dimensions of $2.5 \times 2.5\ mm^2$ were evaporated on the front surface (C-face) of the both wafers. The contacts were made of a 20-nm layer of Cr and a 300-nm layer of Au annealed at 500 °C. The width of the gap between the co-planar contacts was 0.7 mm. The samples with dimensions of $4 \times 9\ mm^2$ were mounted in a vacuum chamber enabling the photocurrent transients to be measured at the temperature range of 320–630 K. The photocurrent transients were generated by a semiconductor laser emitting the UV radiation beam with the wavelength of 375 nm (3.31 eV). The measurements of the transients were made at a photon flux of $\sim 2.8 \times 10^{17}\ cm^{-2}\ s^{-1}$ at the stabilized temperature rising from 320 to 630 K with an increment of 5 K. The duration time of the UV excitation pulses was 1 or 5 ms and the repetition period was 500 ms. The voltage applied between the co-planar electrodes was 20 V. The properties and concentrations of deep-level defects were derived from the digitally recorded photocurrent relaxation waveforms using the two-dimensional numerical analysis with the implementation of the correlation procedure and the inverse Laplace transform algorithm [14,30,31]. This algorithm, implemented in the CONTIN program, allowed distinguishing the defect centres located in two inequivalent lattice sites (hexagonal *h* and cubic *k*). The results of HRPITS measurements showing the defect structure of the A and B wafers of HP SI 4H–SiC are presented in Fig. 14.

The results shown in Fig. 14 indicate that defect structure of real SI 4H–SiC crystals is more complex than that assumed for the modelling. This is because the point defects of the same chemical nature are located in the *h* and *k* lattice sides and have slightly different activation energies. In the material not subjected to the heat treatment (wafer A), we have detected 10 deep traps with activation energies ranging from 555 to 1455 meV. These traps are labelled as: TP1 (555 meV), TP2 (580 meV), TP3 (600 meV), TP4 (615 meV), TT3 (905 meV), TT4 (935 meV), TT5 (1030 meV), TT6 (1125 meV), TP5 (1415 meV), TP6 (1455 meV) and are tentatively attributed to ID9 centre, V_C – related D centre, Z_1 centre ($V_C{}^kV_{Si}{}^h$), Z_2 centre ($V_C{}^hV_{Si}{}^k$), $V_{Si}{}^h$ (3–/2–), $V_{Si}{}^k$ (3–/2–), $V_{Si}{}^h$ (2–/–), $V_{Si}{}^k$ (2–/–), $V_{Si}{}^h$ (–/0), $V_{Si}{}^k$ (–/0), respectively [32,33]. In the annealed material (wafer B), there are 8 deep traps with activation energies ranging from 750 to 1180 meV. The detected traps are labelled as: TT1 (750 meV), TT2 (825 meV), TT3 (905 meV), TT4 (935 meV), TT5 (1030 meV), TT6 (1125 meV), TT8 (1145 meV), TT7 (1180 meV) and are tentatively identified with the following point defects: $V_C{}^hC_{Si}{}^h$ (2–/–), $V_C{}^kC_{Si}{}^k$ (2–/–), $V_{Si}{}^h$ (3–/2–), $V_{Si}{}^k$ (3–/2–), $V_{Si}{}^h$ (2–/–), $V_{Si}{}^k$ (2–/–), $V_C{}^hC_{Si}{}^h$ (–/0), $V_C{}^kC_{Si}{}^k$ (–/0), respectively [32,33].

The properties and concentrations of deep-level defects illustrated in Fig. 14 evidently show that the high-temperature annealing results in the significant changes in the HP SI 4H–SiC defect structure. It leads to disappearing of centres related to carbon vacancies (TP1 and TP2) as well as to annealing out the Z_1 and Z_2 centres formed by divacancies V_CV_{Si}. On the other hand, the centres attributed to silicon vacancies (TT3, TT4, TT5 and TT6) are observed in the annealed material with the concentrations sub-

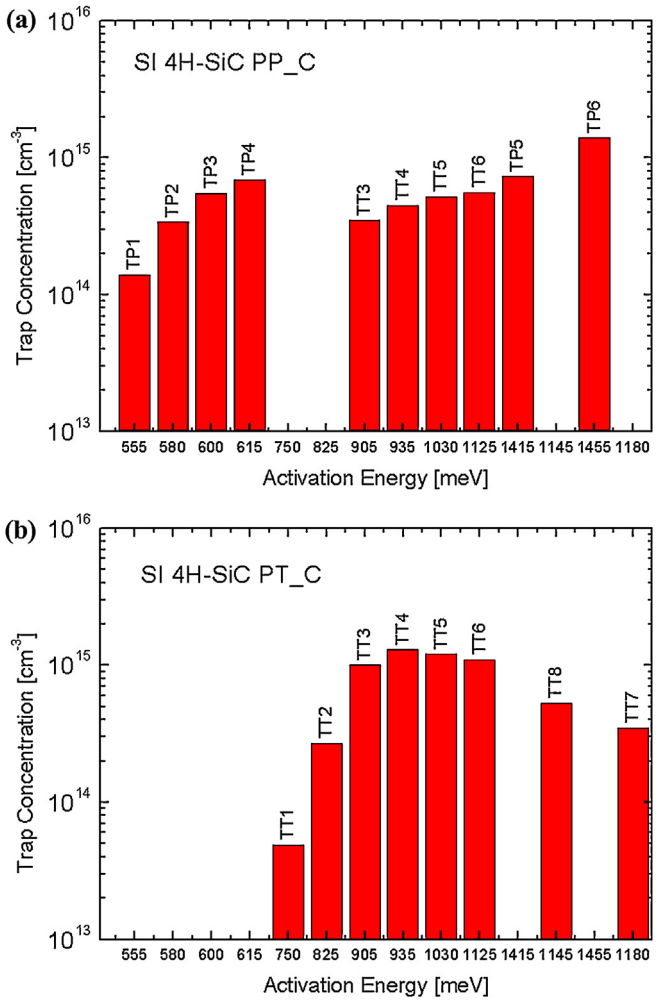

Fig. 14. Concentrations of defect centres detected in a HP SI 4H–SiC wafers: not subjected to the heat treatment at 1670 °C (wafer A) (a), and subjected to the heat treatment at 1670 °C (wafer B) (b). The activation energies of the centres are given on the horizontal axis.

stantially higher than that in the material not subjected to the heat treatment. Moreover, the complexes involving carbon antisites, observed as the TT1, TT2, TT7 and TT8 deep traps, are formed. All these experimental facts allow us to conclude that during the heat treatment at 1670 °C the material becomes strongly C-rich due to the Si sublimation process. In other words, the changes in the 4H–SiC stoichiometry involve the transformations of point defects observed as the deep traps.

Fig. 15 shows the comparison of the photocurrent transients recorded at $T = 320$ K for the A and B HP SI 4H–SiC wafers having deep-level defects with different properties. The transients were induced by the UV excitation with a photon energy of 3.31 eV and a flux of 1.6×10^{17} s^{-1} cm^{-2}. For the both kinds of wafers, the time evolution of the photocurrent pulses is clearly seen. In view of the modelling results, either the photocurrent rise or the photocurrent decay in the wafer A is predominantly affected by the involvement of the Z_1 and Z_2 centres in the capture of excess charge carriers or their thermal emission, respectively. For the annealed material (wafer B), without the Z_1 and Z_2 centres, both the rise and decay of the photocurrent transient are much faster.

The photocurrent pulse is also significantly higher compared to that in the A wafer not subjected to the annealing. This fact means that the Z_1 and Z_2 centres act as recombination centres decreasing the lifetime of excess charge carriers. The presented experimental results are of a great importance for technology of photoconductive

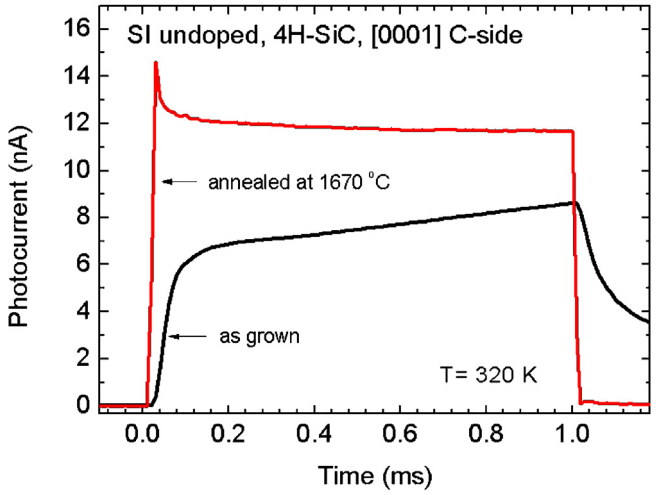

Fig. 15. Comparison of the time evolution of the photocurrent pulses generated by the UV excitation in the A (black curve) and B (red curve) wafers of HP SI 4H–SiC with different properties and concentrations of deep-level defects. The changes in the defect structure of the as-grown material (wafer A) were induced by annealing in a CVD reactor at 1670 °C.

switches based on the SI 4H–SiC. They indicate that for achieving the fast photocurrent pulses in this material it is necessary to substantially diminish the Z_1 and Z_2 centres concentrations. In other words, it is useful to make the SI 4H–SiC strongly C-rich and this can be done by the proper conditions of the heat-treatment.

8. Conclusions

This paper presents a method for modelling the physical processes involving the excess charge carriers capture and emission in semiconductor materials, particularly in SI 4H–SiC single crystals. It was noticed that previously used models were limited to only a small number of defect centres, what resulted in partial understanding of photoconductivity processes. The model presented in this paper considers the main defect centres currently known to occur in the semi-insulating 4H–SiC single crystals. Based on this model, the simulations allow to visualize the time evolution of the excess charge carriers concentrations in the conduction and valence bands at the presence of deep-level defects in the material as well as the kinetics of the capture and emission of excess charge carriers induced by defect centres. Particularly, the simulations have shown that the predominant effect on the transient photoconductivity has the $Z_{1/2}$ centre. This result is also confirmed experimentally by comparing the photocurrent transients generated by the UV excitation pulses in the HP SI 4H–SiC wafers with different deep-level defects. It is demonstrated that the photocurrent pulse is significantly faster and higher in the wafer subjected to a high-temperature annealing producing the strongly C-rich material free of the $Z_{1/2}$ centres. The presented results, obtained either by simulations or experimentally, are of importance for technology of photoconductive switches made of SI 4H–SiC single crystals.

References

[1] W. Shi, C. Maa, L. Hou, G. Xie, L. Tian, S. Wu, Velocity of current filament at the high gain mode of GaAs power photoconductive switches, Physica B 406 (2011) 3741–3744.
[2] M. Missous, Semiconductor material development for terahertz applications, in: Daryoosh Saeedkia (Ed.), Electronic and Optical Materials: Handbook of Terahertz Technology for Imaging, Sensing and Communication, No. 34, Woodhead Publishing Limited, Oxford, Cambridge, Philadelphia, New Delphi, 2013, pp. 464–489.

[3] K. Zhua, D. Johnstonea, J. Leacha, Y. Fua, H. Morkoc, G. Lib, B. Ganguly, High power photoconductive switches of 4H SiC with Si_3N_4 passivation and n^+-GaN subcontact, Superlatt. Microstruct. 41 (2007) 264–270.
[4] I. Jyothi, V. Janardhanam, Jong-Hee Kim, Hyung-Joong Yun, Jae-Chan Jeong, Hyobong Hong, Sung-Nam Lee, Chel-Jong Choi, Electrical and structural properties of Au/Yb Schottky contact on p-type GaN as a function of the annealing temperature, J. Alloys Compd. 688 (2016) 875–881.
[5] Y. Turkulets, T. Bick, I. Shalish, Double surface effect causes a peak in band-edge photocurrent spectra: a quantitative model, J. Phys. D: Appl. Phys. 49 (2016) 365104.
[6] Z. Hemmata, R. Faeza, E. Morenob, F. Rasoulic, F. Radfara, M. Zaimbashi, Transient and steady state study of a rear-illuminated 6H-SiC photoconductive semiconductor switch, Optic 127 (2016) 4615–4620.
[7] C. Longeaud, J.P. Kleider, P. Kaminski, R. Kozlowski, M. Miczuga, Characterization of defect levels in semi-insulating 6H–SiC by means of photoinduced transient spectroscopy and modulated photocurrent technique, J. Phys.: Condens. Matter 21 (2009) 045801.
[8] M. Kato, Y. Mori, M. Ichimura, Microwave reflectivity from 4H–SiC under a high-injection condition: impacts of electron–hole scattering, Jpn. J. Appl. Phys. 54 (2015), 04DP14.
[9] J.S. Sullivan, Wide Bandgap Extrinsic Photoconductive Switches, UNT Digital Library, Livermore, CA, 2013.
[10] D. Chaussende, P.J. Wellmann, M. Pons, Status of SiC bulk growth processes, J. Phys. D: Appl. Phys. 40 (2007) 6150–6158.
[11] T.P. Chow, M. Ghezzo, SiC power devices, MRS Proc. 423 (1996) 9–21.
[12] T. Kimoto, S. Nakazawa, K. Hashimoto, H. Matsunami, Reduction of doping and trap concentrations in 4H–SiC epitaxial layers grown by chemical vapor deposition, Appl. Phys. Lett. 79 (17) (2001) 2761–2763.
[13] K. Fujihira, T. Kimoto, H. Matsunami, High-purity and high-quality 4H–SiC grown at high speed by chimney-type vertical hot-wall chemical vapor deposition, Appl. Phys. Lett. 80 (9) (2002) 1586–1588.
[14] P. Kamiński, R. Kozłowski, M. Miczuga, M. Pawłowski, M. Kozubal, M.a. Pawłowski, High-resolution photoinduced transient spectroscopy of defect centres in vanadium-doped semi-insulating SiC, J. Mater. Sci.: Mater. Electron. 19 (2008) S224–S228.
[15] V.A. Il'in, V.S. Ballandovich, EPR and DLTS of point defects in silicon carbide crystals, Defect Diff Forum 103–105 (1993) 633–644.
[16] M. Wichtowski, Perturbative approach to space–charge field dynamics in photorefractive semiconductors, J. Opt. A 14 (2012), 045201.
[17] M. Lades, Modelling and simulation of wide bandgap semiconductor devices: 4H/6H-SiC Selected Topics of Electronics and Micromechatronics, vol. 3, Shaker Verlag, Aachen, 2000.
[18] N. Schüler, T. Hahn, S. Schmerler, S. Hahn, K. Dornich, J.R. Niklas, Simulations of photoconductivity and lifetime for steady state and nonsteady state measurements, J. Appl. Phys. 107 (6) (2010), 064901.
[19] K. Kelkar, C. Fessler, W.C. Nunnally, N.E. Islam, Experimental and simulation characterization of semi-insulating 6H SIC photoconductive switch for pulsed power applications, Proc. IEEE Pulsed Power Conf. (2005) 904–907.
[20] M. Mubashshir, H. Farooqi, R.K. Srivastava, Structural, optical and photoconductivity study of ZnO nanoparticles synthesized by annealing of ZnS nanoparticles, J. Alloys Compd. 691 (2017) 275–286.
[21] P. Tierney, T.J. Ennis, Á. Allen, J. Wright, The role of mid-band gap defect levels in persistent photoconductivity in RF sputtered SnO_2 thin films, Thin Solid Films 603 (2016) 50–55.
[22] M. Suproniuk, P. Kamiński, R. Kozłowski, M. Pawłowski, Effect of deep-level defects on transient photoconductivity of semi-insulating 4H–SiC, Acta Phys. Pol. A 125 (4) (2014) 1042–1048.
[23] M. Kozubal, Institute of Electronic Materials Technology, Warsaw, Ph.D. thesis, 2011.
[24] K. Danno, T. Kimoto, Deep hole traps in as-grown 4H–SiC epilayers investigated by deep level transient spectroscopy, Mater. Sci. Forum 527–529 (2006) 501–504.
[25] M.E. Zvanut, V.V. Konovalov, The level position of a deep intrinsic defect in 4H–SiC studied by photoinduced electron paramagnetic resonance, Appl. Phys. Lett. 80 (3) (2002) 410–412.
[26] P. Kamiński, M. Kozubal, J.D. Caldwell, K.K. Kew, B.L. VanMil, R.L. Myers-Ward, C.R. Eddy Jr., D.K. Gaskill, Deep-level defects in epitaxial 4H–SiC irradiated with low-energy electrons, Electron. Mater. 38 (3/4) (2010) 26–34.
[27] M. Suproniuk, et al., An intelligent measurement system for diagnosing of semi-insulating materials by photoinduced transient spectroscopy, Electr. Rev. 85 (11) (2009) 93–98.
[28] M. Suproniuk, et al., An intelligent measurement system for characterisation of defect centres in semi-insulating materials, Electr. Rev. 86 (11a) (2010) 247–252.
[29] R.H. Bube, Photoelectric Properties of Semiconductors, Cambridge University Press, Cambridge, UK, 1992.
[30] R. Kozłowski, P. Kamiński, J. Żelazko, Determining the defect centre concentration in high-resistivity semiconductors from the Laplace spectral fringes obtained by the analysis of the photocurrent relaxation waveforms, Electr. Mater. (ITME) 40 (2012) 19–33.
[31] J. Krupka, W. Karcz, S.P. Avdeyev, P. Kamiński, R. Kozłowski, Electrical properties of deuteron irradiated high resistivity silicon, Nucl. Instr. Meth. Phys. Res. B 325 (2014) 107–114.
[32] N.T. Son, P. Carlsson, J. ul Hassan, B. Magnusson, E. Janzén, Defects and carrier compensation in semi-insulating 4H–SiC substrates, Phys. Rev. B 75 (2007) 155204.
[33] M.V.S. Chandrashekhar, I. Chowdhury, P. Kaminski, R. Kozlowski, P.B. Klein, T. Sudarshan, High purity semi-insulating 4H–SiC epitaxial layers by defect-competition epitaxy: controlling Si vacancies, Appl. Phys. Expr. 5 (2012) 025502.